BIOCHEMISTRY
including biophysical chemistry & molecular biology

Article

pubs.acs.org/biochemistry

Characterization of Unfolding Mechanism of Human Lamin A Ig Fold by Single-Molecule Force Spectroscopy—Implications in EDMD

Manindra Bera,[†] Hema Chandra Kotamarthi,[¶] Subarna Dutta,[†] Angana Ray,[‡] Saptaparni Ghosh,[†] Dhananjay Bhattacharyya,[‡] Sri Rama Koti Ainavarapu,[¶] and Kaushik Sengupta*[,†]

[†]Biophysics & Structural Genomics Division, Saha Institute of Nuclear Physics, 1/AF, Bidhannagar, Kolkata, West Bengal 700064, India

[‡]Computational Science Division, Saha Institute of Nuclear Physics, 1/AF, Bidhannagar, Kolkata, West Bengal 700064, India

[¶]Department of Chemical Sciences, Tata Institute of Fundamental Research, Mumbai, Homi Bhabha Road, Mumbai, Maharashtra 400005, India

ABSTRACT: A- and B-type lamins are intermediate filament proteins constituting the nuclear lamina underneath the nuclear envelope thereby conferring proper shape and mechanical rigidity to the nucleus. Lamin proteins are also shown to be related diversely to basic nuclear processes. More than 400 mutations in human lamin A protein alone have been reported to produce at least 11 different disease conditions jointly termed as laminopathies. These mutations in lamin A are scattered throughout its helical rod domain, as well as the C-terminal domain containing the conserved Ig-fold region. The commonality of phenotypes in all these diseases is characterized by misshapen nuclei of the affected tissues which might stem from altered rigidity of the supporting lamina hence lamins. Here we have focused on autosomal dominant Emery−Dreifuss Muscular Dystrophy, one such laminopathy where R453W is the causative mutation located in the Ig domain of lamin A. We have investigated by single-molecule force spectroscopy how a stretching mechanical perturbation senses the destabilizing effect of the mutation in the lamin A Ig domain and compared the mechanoelastic properties of the mutant R453W with that of the wild-type in conjunction with steered molecular dynamics. Furthermore, we have shown the interaction of Ig domain with emerin, another key player and interacting partner in the pathogenesis of EDMD, is disrupted in the R453W mutant. This altered mechanoresistance of Ig domain itself and consequent uncoupling of lamin A-emerin interaction might underlie the altered mechanotransduction properties of EDMD affected nuclei.

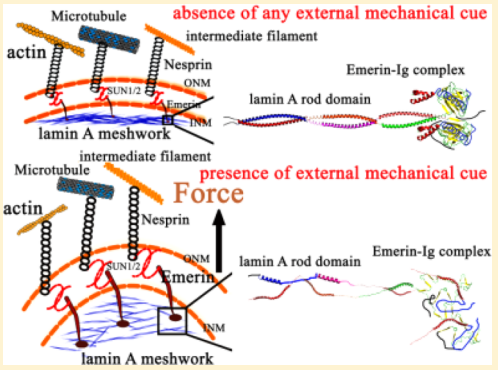

Lamins are type V intermediate filament proteins present as "fibrous lamina"[1] in the nucleus of metazoan cells except plants and confer proper shape and rigidity to the nucleus. A- and B-type lamins encoded by LMNA and LMNB1/LMNB2 genes, respectively, constitute the nuclear lamins. Like all other intermediate filament proteins, lamins form basic coiled-coil dimers at the initial stage of assembly which progressively self-assemble into higher order structure by parallel stacking interaction.[2,3] The higher-order structure culminates into distinct networks of A and B type lamins in the nucleus,[4] which acts a supporting scaffold for the nuclear envelope and also provide site of attachments for other nuclear proteins. The lamins possess a short N-terminal head domain followed by a long coiled-coil forming central alpha helical region and a relatively long unstructured C-terminal domain.[5−7] The C-terminal domain of lamin proteins contains a highly conserved motif containing nine β-sheets similar to a type s immunoglobulin fold (Ig-fold).[8,9] This motif is the site of interaction between different nuclear factors, as well as controls homotypic and heterotypic lamin interactions to promote assembly of the protofilament to form 10 nm filaments.[10−13] Lamin A network is the principal mechanoelastic component of the nucleus in a differentiated cell,[14,15] which responds to external mechanical stimuli transmitted to the nucleus through the Linker of Nucleoskeleton and Cytoskeleton (LINC) complex.[16−18] External stimuli include a wide range of cellular processes like alteration of extracellular matrix, cellular migration/trafficking and differentiation. How exactly such stimuli register changes in the supramolecular reassembly of lamin proteins is an enigma. The lamina is in close connection to the nuclear envelope which is mediated by noncovalent interactions with membrane proteins. Numerous nuclear envelope proteins, for instance emerin, SUN 1, and LAP 2β, have been identified[19−22] to be coupled to the nuclear lamina. These interactions play pivotal roles in the transmission of external forces via LINC complex.[23,24] Emerin is such an integral membrane protein that extends into the nucleoplasmic space.[25] Early reports indicated that lamins colocalized with

Received: June 11, 2014
Revised: October 17, 2014
Published: October 24, 2014

   dx.doi.org/10.1021/bi500726f | *Biochemistry* 2014, 53, 7247−7258

emerin during mitosis.[26] Furthermore, the distribution of emerin closely coincides with that of lamin A and differed from B-type lamins.

Lamins have gained immense importance since the past decade due to the discovery of a plethora of diseases termed as laminopathies which are caused by mutations in lamin proteins particularly lamin A. Laminopathies include Hutchinson Gilford Progeria Syndrome (HGPS), Emery-Dreifuss Muscular Dystrophy (EDMD), Dilated Cardiomyopathy (DCM), Familial Partial Lipodystrophy (FPLD), Duchene Muscular Dystrophy (DMD), Atypical Werner's Syndrome to name a few among 11 different diseases.[27−29] All of these result from about 400 mutations (www.umd.be/LMNA)[30] in the LMNA gene alone. A major hallmark of most laminopathies is altered nuclear morphology which includes phenotypes like blebbing, herniations and elongated nuclei.[12,31] This means the nuclei under diseased conditions have attenuated strain bearing capacity thereby resulting into distortions. EDMD is one such severe disease which is characterized by progressive weakness and wasting of skeletal muscles which ultimately result into premature contractures of Achilles tendons and cardiac diseases associated with conduction defects. Analysis of primary fibroblasts from patients suffering from EDMD showed dysmorphic nuclei with abnormal staining patterns for lamin A and emerin.[32] X-linked EDMD is caused by mutations in emerin, whereas autosomal dominant EDMD results from mutations in lamin A protein. Therefore, it is easy to conjecture that mutant lamin A thereof might form a meshwork with altered elasticity which can bear less strain and hence resulting into misshapen nuclei. In retrospect, the altered viscoelastic behavior of the lamin A protein has been elucidated recently with dilated Cardiomyopathy mutants[15] where the mutant protein networks were shown to be less robust and yielding to lower strain compared to wild type protein.

Taking cues from these findings we have focused on one such mutation leading to EDMD which is localized in the Ig fold of lamin A protein. Previous studies have emphasized the importance of this domain and likewise the structure has been solved by NMR and X-ray crystallography.[8,9] Interaction of Ig domain with Proliferating Cell Nuclear Antigen (PCNA) and its implication in replication had been shown;[13] interaction of Ig domain with emerin also had been mapped[33] to great details. So, we reasoned to uncover how the mechanoelastic behavior Ig domain of lamin A might be altered at the single molecule level as a sequel to mutation therein which as an ensemble might perturb the strain bearing property of the network. We have chosen R453W mutation in the Ig domain which causes autosomal dominant Emery−Dreifuss Muscular Dystrophy (EDMD).[34,35] The rationale behind choosing this mutation is the highly conserved nature of the site within Ig domain across the invertebrate and vertebrate species.[36] This mutation was shown to disrupt two salt bridges in the lamin A Ig domain.[9] In AFM pulling experiments, we characterized the force−extension profiles of the Ig domains using titin I27 domain as the reference signature molecule. Subsequent pulling experiments with LA R453W Ig (mutant) showed interesting differences in unfolding behavior compared to the wild type (LA wt Ig) which was also elucidated from steered molecular dynamics simulation. However, no significant difference in unfolding behavior was registered from similar experiments performed in the presence of emerin, whereas significant differences in the binding affinity of LA R453W Ig and emerin were registered from SPR and solid phase binding assays. Taken together we concluded that the physical interaction of Ig domain with emerin and force induced stretching of Ig domain could be connected by a cause and effect relationship. Proximity of the lamin Ig fold to emerin and its binding strength determines the coupling and propagation of any mechanical stimulus from cytoplasm to nuclei which in turn results in the stretching of Ig fold strands. The resultant stretching thereby alters the nuclear elasticity.

EXPERIMENTAL PROCEDURES

Site-Directed Mutagenesis. Single amino acid mutations were performed as described by Bhattacharjee et al.[7] using Site-Directed Mutagenesis Kit (Stratagene) and *LMNA*-R453W_sense 5′-*GGAGGGCAAGTTTGTCTGGCTGCGCAA-CAA*-3′, *LMNA*-R453W_antisense 5′-*TTGTTGCGCAGCCA-GACAAACTTGCCCTCC*-3′ primers from Sigma-Aldrich. The mutation was confirmed by Sanger sequencing (Excelris, India).

Cloning, Expression, and Purification. $(I27\text{-}LA\ wt\ Ig)_4$ and $(I27\text{-}LA\ R453W\ Ig)_4$ cassettes were inserted into pQE-80L in an alternative fashion by iterative cloning method.[37] Forward primer 5′-*CGCGGATCCGCGAGCAGCTTCTCACAGCAC-GCACGCACTAGC*-3′ and reverse primer 5′-*CGGGGTACC-CCGTTAGGAAGATCTTCCGTCCTCAACCACAGTCACTG-AGCG*-3′ were used to amplify the LA wt Ig and LA R453W Ig fragments using Phusion High-Fidelity DNA Polymerase (Thermo Scientific Inc., USA) The forward and reverse primers contained a *Bam*HI restriction site and a tandem *Bgl*II, a stop codon, *Kpn*I site, respectively. PCR products were digested with *Bam*HI-HF and *Kpn*I-HF {New England Biolabs (NEB), USA} and gel purified using Gel Extraction Kit (Qiagen, Netherlands). pQE-80L vector containing I27 monomer cassette[38] was similarly digested with *Bgl*II and *Kpn*1-HF restriction enzymes (NEB) followed by ligation using T4 DNA Ligase (NEB) at 16 °C overnight. After transformation in XL-1Blue cells, positive clones were selected by colony PCR. Successive iterations were performed to generate the dimer and tetramer cassettes. The same methods were followed to construct $(I27\text{-}LA\ R453W\ Ig)_4$. LA wt Ig and LA R453W Ig monomer units were amplified using above-mentioned primer sets and subsequently cloned in a one-step method into pQE-80L (Qiagen) vector as described above. Plasmids containing the appropriate insert sequences were confirmed from Sanger sequencing data. Thereafter, all plasmids were transformed into BL21 (DE3) pLysS cells and induced with 1 mM IPTG at an OD_{600} of 0.5 for 6 h at 37 °C for protein expression. Cell pellets were lysed with 25 mM Tris-HCl (pH 7.4), 150 mM NaCl, 1 mM DTT, 1% Triton-X 100. Proteins were purified to near homogeneity over His-trap column (GE Healthcare Biosciences, USA) and resolved on 4−20% SDS-PAGE followed by Coomassie staining. Final protein stocks were dialyzed against 25 mM Tris-HCl (pH 7.4), 150 mM NaCl to remove imidazole. Emerin protein was expressed from pET-15b and/or pET-21 received as gifts from Dr. James Holaska, University of Chicago and Dr. Frank Bernhard, J.W. Goethe University of Frankfurt. Emerin was purified by (Superdex 16/60 200 G Gel Filtration column (GE Healthcare) using 25 mM Tris-HCl (pH 7.4), 150 mM NaCl, 1 mM DTT, 6 M urea as column buffer. Subsequently the protein was renatured by removing urea by step dialysis. Protein concentrations were routinely checked with Bradford reagent (Bio-Rad, USA).

Differential Scanning Calorimetry (DSC). Thermal denaturation profiles of all the proteins were measured in 25

mM Tris-HCl (pH 7.4), 150 mM NaCl, in a VP-DSC Micro calorimeter (Microcal, LLC, and Northampton, MA). A 10−50 μM sample was analyzed in each case between 16 and 80 °C for LA wt Ig monomer, titin I27 monomer, (I27-LA wt Ig) tetramer and (I27-LA R453W Ig) tetramer and between 16 and 65 °C for LA R453W Ig monomer, at a scan rate 30 °C/h. at approximately 30 psi pressure. Prior to measurement, the instrument was thermally stabilized by multiple buffer scans. All the resulting thermograms were analyzed by in-built VP Viewer software with Origin 7.0.

Solid-Phase Binding Assay and Western Blot. In this method 5−10 μg (∼0.4 nmole -0.8 nmole) of LA wt Ig and LA R453W Ig were spotted on nitrocellulose membrane and incubated overnight at 4 °C with 20−25 μg (∼0.6 nmole -0.73 nmole) of emerin in protein incubation buffer comprising of 25 mM Tris-HCl, pH 7.4, 150 mM NaCl. The membrane was then washed with PBS-0.1% Tween 20 and probed with goat anti-emerin antibody (C-20, Santa Cruz Biotech Inc. USA) at a dilution of 1:100 followed by bovine anti-goat HRP conjugated secondary antibody (Santa Cruz) at 1:1000 dilution. The blots were developed by chemiluminescence using Supersignal Westpico Chemiluminescent substrate (Thermo Scientific, USA). Expressions of Ig proteins were verified by blotting with anti-His antibody (gift from Dr. Oishee Chakrabarti, Saha Institute of Nuclear Physics, Kolkata) at a dilution of 1:1500 and similar dilution for secondary antibody. Intensity profiles of the dot blots, repeated at least in triplicates were quantified by ImageJ version 1.47 after appropriate normalization and plotted as bar diagrams.

Single-Molecule Force Spectroscopy (SMFS). All single-molecule force spectroscopy pulling experiments were performed on a custom-built atomic force microscope (AFM) as described by Kotamarthi et al.[39] We used both Bruker and Olympus Biolever cantilevers. The spring constants of the cantilevers were calculated to be ∼40 pN/nm for the Bruker and ∼20 pN/nm for the Olympus Biolever in the buffer, respectively. The concentrations of protein solutions used in the experiments varied from 2 μM to 8 μM. In pulling experiments for protein−protein interaction measurements protein and ligand were used in 1:4 molar ratios, and before any measurements protein samples were incubated for at least 1 h at room temperature, followed by a centrifugation step at 13000 rpm for 5 min. All the forces versus extension (FX) traces were recorded at a pulling speed of 1000 nm/s. All the experiments were performed in buffer containing 25 mM Tris-HCl, pH 7.4, 150 mM NaCl at 25 °C.

Data Analysis. The worm-like chain model of polymer elasticity[40] was used to fit the FX traces with eq 1

$$F(x) = \frac{k_B T}{p}\left[\frac{1}{4}\left(1 - \frac{x}{L_c}\right)^{-2} - \frac{1}{4} + \frac{x}{L_c}\right] \quad (1)$$

where p, L_c, k_B, and T denote persistence length, contour length, Boltzmann constant, and absolute temperature, respectively. All the F-X traces were analyzed in Igor Pro 6.02 from WaveMetrics, USA.

Surface Plasmon Resonance (SPR). Protein−protein interaction kinetics was analyzed on Biacore X-100 using NTA chip (Biacore, GE Healthcare Biosciences, USA). Initially 1 mM $NiSO_4$ was passed over the NTA-chip at 10 μL/min flow rate for 60 s followed by the His-tagged protein which was also passed for 60 s at 20 μL/min flow rate to bind to the Ni-NTA chip. One μM of monomeric proteins and 0.5 μM of tetrameric proteins respectively were immobilized on the chip and the buffer was run for 60 s at 10 μL/min flow rate while 0.5−4.0 μM emerin was passed at 10 μL/min flow rate with 60 s contact time and dissociation time using flow cell 2. At the end of each binding chip was regenerated using 0.5 M EDTA for 30 s at 10 μL/min flow rate. Kinetic analyses were performed by the inbuilt evaluation software.[41] All the experiments were carried out at least three times or more in 25 mM Tris-HCl, pH 7.4, 150 mM NaCl at 25 °C.

Steered Molecular Dynamic (SMD) Simulations. Equilibrium molecular dynamics simulations for both the wild-type and the mutant proteins were carried out using NAMD 2.9 software[42] with CHARMM-22 force field.[43] Crystal structure of the C-terminal of lamin A Ig domain (PDB ID 1IFR) was considered as the initial structure of the native protein and the coordinates of the mutant protein were generated using Modeller 9.11.[44] In each simulation, the protein molecules were explicitly solvated by TIP3P water molecules and charge neutralizing Cl^- ions in a periodic box whose boundaries extended at least 10 Å from any solute atom. These two systems were energy minimized using CHARMM.[45] Particle Mesh Ewald (PME) summation method was used to treat the long-range electrostatic interactions. A force switch method was applied for nonbonded interactions with 12 Å cutoff. After energy minimization the systems were gently heated to 300 K in 30 ps. This process was followed by equilibrium molecular dynamics simulation in explicit solvent and steered molecular dynamics simulation with implicit solvent model. The equilibrium molecular dynamics had a final production run of 100 ns by Constant Pressure Temperature (CPT) dynamics algorithm at 1 atm pressure, with 1.0 fs time step.

Steered Molecular Dynamics Simulations[46−48] were carried out with Generalized Born Implicit Solvent (GBIS) model for water[49−51] on the wild-type protein and its mutant. Simulations were performed with a time step of 1 fs, a solvent dielectric constant of 78.5, and a cutoff of Coulomb forces with a switching function starting at a distance of 15 Å and reaching zero at 16 Å. SMD simulations of constant velocity stretching (SMD-CV protocol) were carried out by fixing the C-alpha atom of N-terminal residue (res id: 432) and applying external forces to the C-alpha atom of C-terminal residue (res id: 544) which is the SMD atom, along the direction of the vector from residue 432 to residue 544. In such simulations the SMD atom is attached to a dummy atom via a virtual spring. This dummy atom is then moved at a constant velocity. The force experienced by the pulled terminal atom, F is

$$F = k(vt - x) \quad (2)$$

where, x is the displacement of the pulled atom from its original position, v is the pulling velocity, and k is the spring constant. Force was applied on the dummy atom with a virtual spring of spring constant 0.6 kcal/mol/Å^2 and pulling velocity 0.0000025 Å/fs parallel to the hydrogen bonds of first β-sheet. The simulation trajectory was made up by frames collected every 1.0 ps and then analyzed. Secondary structure analysis of the simulation snapshots was done following DSSP algorithm[52]as implemented in CHARMM software along with plotting the contact maps for protein structures obtained from equilibrium Molecular Dynamics Simulation trajectories.

dx.doi.org/10.1021/bi500726f | Biochemistry 2014, 53, 7247−7258

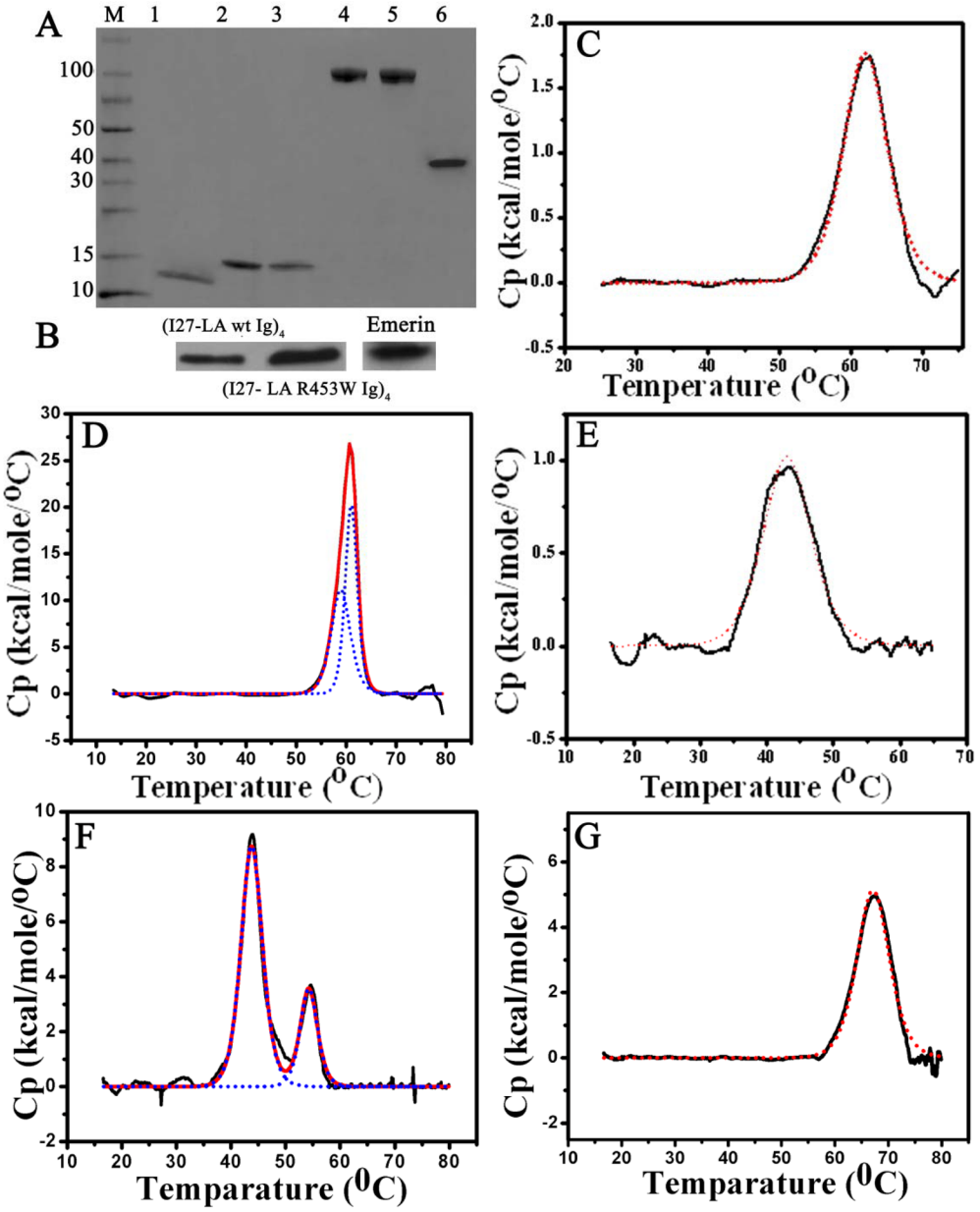

Figure 1. Characterization of the chimeric constructs using gel electrophoresis. (A) 4−20% gradient gel separation of titin I27 monomer, lamin A wild type Ig monomer (LA wt Ig), R453W Ig monomer (LA R453W Ig), $(I27\text{-}LA\ wt\ Ig)_4$, $(I27\text{-}LA\ R453W\ Ig)_4$ and emerin in lanes 1, 2, 3, 4, 5, and 6 respectively. Bands of the marker represented in kilo Daltons are represented at the side of the panel. (B) Immunoblot analysis of the tetrameric constructs with anti-His antibody and emerin with anti-emerin antibody. Corresponding thermal denaturations were performed using differential scanning calorimetry on wild type lamin A/C Ig domain (C), R453W Ig domain (E), I27 monomer (G), $(I27\text{-}LA\ wt\ Ig)_4$ (D), and $(I27\text{-}LA\ R453W\ Ig)_4$ (F). In both monomeric and I27 containing tetrameric proteins lamin wild type and R453W Ig domain were unfolded at 61.9 ± 0.02 °C and 43.8 ± 0.03 °C respectively. All the experiments were performed in buffer containing 25 mM Tris-HCl, 150 mM NaCl, pH 7.4. The observed data (black line) were deconvoluted (blue line) using the in-built VP Viewer software with Origin 7.0. The red curves denote overall fit of the data.

RESULTS

Protein Expression and Purification. Heterologous overexpressions of the proteins were achieved in 2xYT medium. The proteins were purified to near homogeneity by using FPLC. The protein fractions were analyzed on a 4−20% gradient or 10% SDS polyacrylamide gels as appropriate and blotted with anti-His antibodies for Ig constructs and antiemerin antibody for emerin (Figure 1A). Pooled fractions were concentrated by using Amicon concentrators with molecular cut offs between 3 and 10 kDa. It was ensured that proteins of similar purities were used for repeating the experiments under identical conditions. For all subsequent experiments described hereafter, the protein solutions were routinely centrifuged at room temperature at 13000 rpm for at least 10 min to remove any suspended particles that might arise from particulate precipitates if any. However, we never observed any out-of-phase behavior for any protein used in this study. We hereby adopt the convention of referring to the LA Ig-domain and $(I27\text{-}LA\ Ig)_4$ as monomer and tetramer, respectively. Therefore, we have mentioned the wild type and mutant constructs as $(I27\text{-}LA\ wt\ Ig)_4$ and $(I27\text{-}LA\ R453W\ Ig)_4$ respectively in the text.

dx.doi.org/10.1021/bi500726f | Biochemistry 2014, 53, 7247−7258

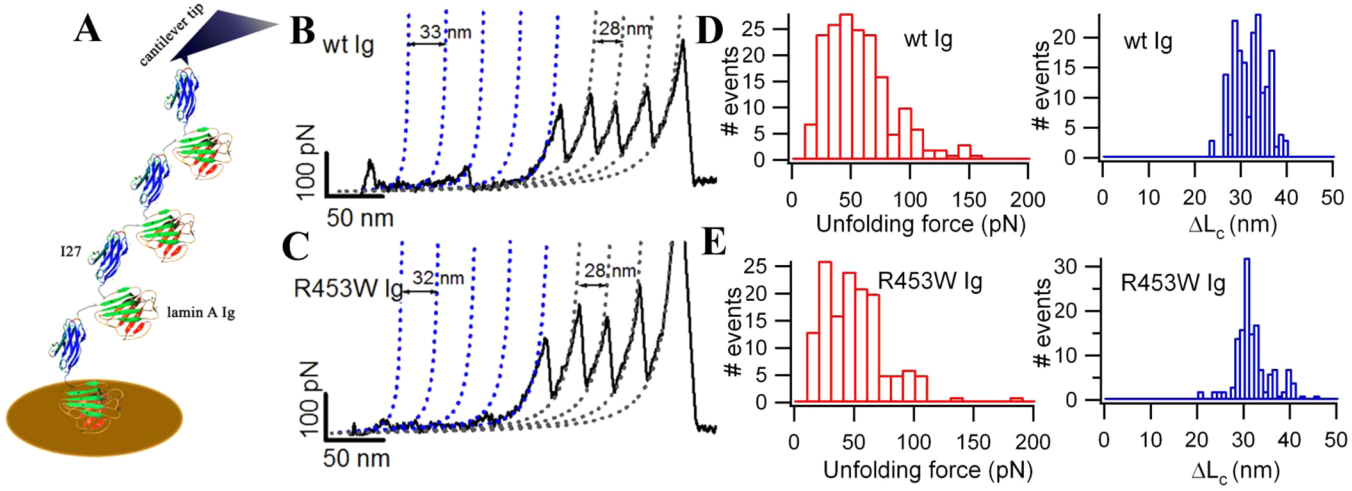

Figure 2. Mechanical unfolding of the wild type and mutant lamin Ig domains in SMFS experiments. (A) Cartoon diagram showing the stretching of tetrameric constructs of the proteins being pulled from the gold coated coverslip by AFM cantilever tip. In this construct four titin I27 and lamin Ig fold domains were placed in an alternating fashion. (B) Representation of force versus extension traces of the wild-type Ig domain, where Ig domains were unfolding at lower force (~56 pN) with increase in contour length (ΔL_c) of 32 nm compared to titin I27 which unfolded at higher force with 28 nm increments in contour length. Red and blue histograms (D) depicted the events (n = 180) for unfolding force and change in contour length, respectively. (C) Representative force−extension curve for the R453W Ig fold mutant. Mutant domains were unfolding at ~49 pN forces with 32 nm increase in contour length. Red and blue histograms (E) similarly depicted unfolding events and the increase in contour length (ΔL_c) respectively (n = 143). All the force extension curves were fitted by WLC model, where blue fitting dots are denoting for lamin wt Ig/R453W Ig domain and gray dots for I27domains. Scale bars showing unfolding force and increase in contour length are 100 pN and 50 nm, respectively.

Analysis of Thermal Stability of (I27-LA wt Ig/R453W Ig)$_4$. Differential scanning calorimetry is a precise method to determine the thermal stability of protein and its corresponding unfolding behavior. These studies helped us to detect any possible alteration of the lamin A Ig domain structure due to the introduction of the I27 domain into the structure. The monomer of LA wt Ig and LA R453W Ig showed significantly different denaturation temperatures of 62 and 43 °C respectively as reported earlier from thermostability analysis by CD.[9] To check any deleterious effect of I27 on the lamin Ig domains we performed the same thermal unfolding experiments with the tetrameric constructs (Figure 1). For (I27-LA wt Ig)$_4$ polyprotein we obtained a single transition point at 62 °C whereas (I27-LA R453W Ig)$_4$ exhibited two distinct transition points at 43 and 56 °C. Hence, we concluded that the thermal stability of LA wt Ig/LA R453W Ig was unaltered and I27 did not affect the native folding of the Ig domains. The transition point of 56 °C in mutant construct could be attributed to I27. Although single I27 unit unfolded at 67 °C (Figure 1G), the transition point merged with that of the Ig domain in the construct (I27-LA wt Ig)$_4$ thereby yielding a single transition point at 62 °C. Therefore, we could establish the fact that introduction of the I27 as a signature moiety did not change the independent native folding of the Ig domains.

Mechanical Unfolding of Lamin Ig Domain and Stability of Ig−Emerin Complex. We performed single-molecule pulling measurements on lamin Ig domains using chimeras (I27-LA wt Ig)$_4$ and (I27-LA R453W Ig)$_4$. In single-molecule force versus extension (F-X) traces I27 serves as a marker protein, whose mechanical properties have been characterized previously.[38,53,54] The unfolding force for the Ig domain was observed to be significantly lower (56 ± 29 pN) than that of I27 (200 ± 30 pN) at 1000 nm/s pulling velocity (Figure 2B and 2C), although both belong to immunoglobulin-like family consisting of nine beta strands packed in beta-sandwich fold. This could possibly be ascribed to the favorable unzipping geometry of the terminal β-strands of lamin Ig domain in contrast to shearing geometry of I27 (Figure 6). Therefore, Ig domains were unfolded first followed by I27. In Figure 2B, first sawtooth pattern with four low force peaks might have arisen from the unfolding events of four lamin Ig domains with ~32 nm spacing in between the adjacent peaks. Subsequent four peaks were due to I27 unfolding corresponding to 28 nm contour length whereas the last peak (>400 pN) resulted from the detachment of the polyprotein from the cantilever tip of the surface. However, it must be noted that we did not always observe clearly all the force peaks of lamin Ig domains expected based on the number of I27 force peaks in a given FX trace. This might be due to their low unfolding force and as a result some of them get buried in the noise level. Nevertheless, the design of the construct and the corresponding contour length analysis ensured the contribution of the lamin A Ig domain in the mechanical stretching. The persistence length values varied between 0.6 ± 0.3 nm for lamin data to get the best fits during the WLC fitting. Because of EDMD causing R453W mutation in the Ig domain, the unfolding force was lowered to 49 ± 27 pN which meant mutant domain was mechanically weaker compared to that of wild type domain. This is in line with the previous results where R453W was demonstrated to have strong destabilizing effects of the structure of Ig domain.[9] Histograms of unfolding force and contour lengths have been shown in Figure 2D and 2E. The results for the signature molecule, I27 completely conformed to the previous reports.[37,53,55,56] From contour length analysis, we obtained the change in contour length as 31.7 ± 3.5 nm for wild type Ig domain and 31.4 ± 4.1 nm for lamin R453W Ig domain instead of the theoretical value of 41 nm (113 × 0.37 − size of the folded structure(0.71)), which could be explained from SMD results discussed subsequently. Summary of unfolding forces and subsequent increase in contour lengths are shown in Table 1.

dx.doi.org/10.1021/bi500726f | Biochemistry 2014, 53, 7247−7258

Table 1. Results from Single-Molecule Mechanical Unfolding Experiments of Lamin A Ig Domain and Its R453W Mutant in Absence and Presence of Emerin[a]

protein	force (pN)	ΔL_c (nm)
LA wt Ig (n = 180)	56 ± 29	31.7 ± 3.5
LA R453W Ig (n = 143)	49 ± 27	31.4 ± 4.1
LA wt Ig + Emerin (n = 64)	45 ± 23	31.0 ± 2.1
LA R453W Ig + Emerin (n = 50)	48 ± 18	31.8 ± 4.4

[a]Unfolding forces and the increase in contour length are obtained from the single-molecule force spectroscopy experiments. Here, n and ΔL_c represent the number of events and the increase in contour length upon unfolding, respectively.

External mechanical cues are transferred to lamin network through cytoskeleton-nucleoskeleton coupling complex[23,24,57] where emerin is an important effector molecule coupled to lamin A.[58,59] Although for this EDMD mutation, nuclei did not show deformability, significant cytoskeletal displacement across the force application site was observed in cultured cells transfected with lamin A mutants.[60] So we intended to look whether emerin augmented any mechanical attributes to lamin Ig fold through a complex formation. We performed the pulling experiment with the same constructs (Figure 2A) in the presence of emerin. On binding with emerin the lamin A Ig domain unfolded at lower force (45 ± 23 pN) compared to the wild type in absence of emerin. But in case of R453W, emerin did not alter the unfolding behavior (Figure 3). The Student's t-test was performed on the unfolding forces of LA wt Ig and its R453W mutant, and their complexes with emerin to verify if the differences observed are statistically significant. The p-value between LA wt Ig and R453W mutant was 0.009 and the p-value between LA wt Ig and its complex with emerin was 0.002. This indicates that the differences between the unfolding forces of LA wt Ig vs R453W mutant and LA wt Ig vs LA wt Ig/emerin complex are statistically significant. On the other hand, the p-value between R453W mutant with and without emerin was 0.5, which makes it statistically insignificant. This we could infer directly from the small change in unfolding force upon emerin binding to R453W mutant. Hence, we are certain that the 13% decrease in the unfolding force of LA wt Ig upon R453W mutation and 20% decrease in the same upon emerin binding are important observations from single-molecule pulling experiments that might have functional implications as discussed the later section.

So, it was evident that as the wild type protein bound emerin more strongly, the unzipping geometry of the Ig domain was changed eventually destabilizing wild type Ig domain in single-molecule AFM studies. As R453W mutant associated with emerin rather loosely, it could not alter the geometry of the H-bond vectors toward destabilization. Hence the unfolding force was not changed significantly for R453W. The biochemical interactions of both the wild type and mutant chimeric constructs with emerin were shown subsequently using SPR and solid phase binding assay (Figure 5). In presence of emerin R453W mutant domain unfolded more or less at same force (48 ± 18 pN), with 31.8 ± 4.4 nm increase in contour length. Sometimes larger peaks were obtained with wild type and the mutants in the presence of emerin. This could be attributed to intrinsic aggregation propensity of emerin. This explains why we got significantly lower number of events: 64 for wild type and 50 for mutant constructs in the presence of emerin. It could be speculated that lamin−emerin interaction might be dictated by surface potential. The electrostatic potential which was mapped using pymol APBS tool, got altered as a sequel to mutation (Figure 6) hence perturbing the interaction with emerin.

Steered Molecular Dynamics (SMD) Simulation. We obtained a noticeable change from single molecule force spectroscopy in the unfolding behavior of lamin A Ig domain because of a single point mutation which is an ensemble of individual domains. The stretching of individual strands on application of force could not be visualized from SMFS and is an important avenue to explore. Therefore, we resorted to steered molecular dynamics (SMD) simulation for unraveling the molecular events pertaining to individual β-strand stretching. Equilibrium MD simulations of the native and

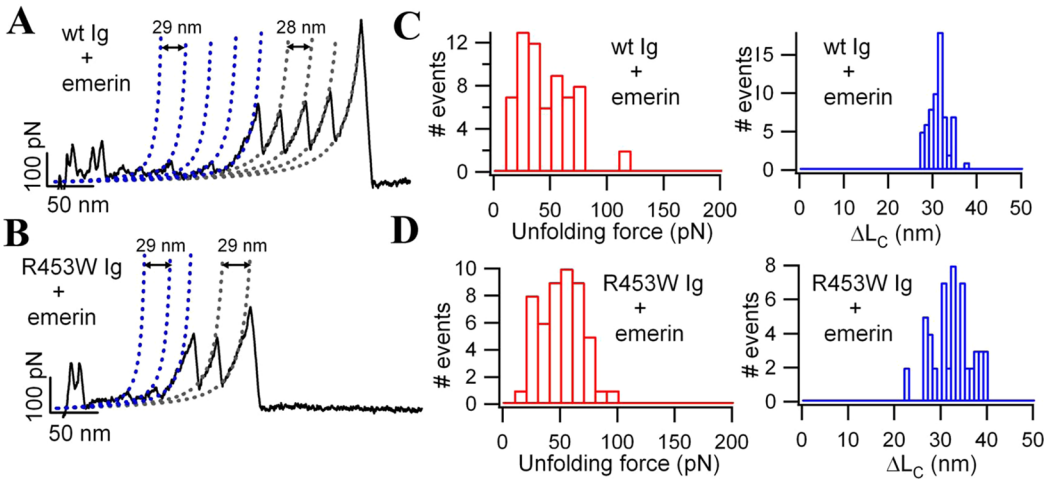

Figure 3. Force vs extension (FX) traces and the statistics of Ig domain−emerin complexes for both wild type and mutant. Representative traces for the (A) wild type Ig domains and (B) R453W Ig unfolding events by SMFS in the presence of emerin, respectively. (C) In presence of emerin lamin A Ig domains were unfolding at ∼45 pN force with ∼31 nm increase in contour length (ΔL_c), (D) force extension trace for the R453W Ig mutant in the presence of emerin. Red and blue histograms in both cases showed the unfolding force and the increase in contour length (ΔL_c) respectively, total no events are 64 and 50, respectively. All the force−extension traces were fitted with WLC model, blue dots are for the fitting of lamin Ig domains in the presence of emerin whereas gray dots are for I27 domains.

dx.doi.org/10.1021/bi500726f | Biochemistry 2014, 53, 7247−7258

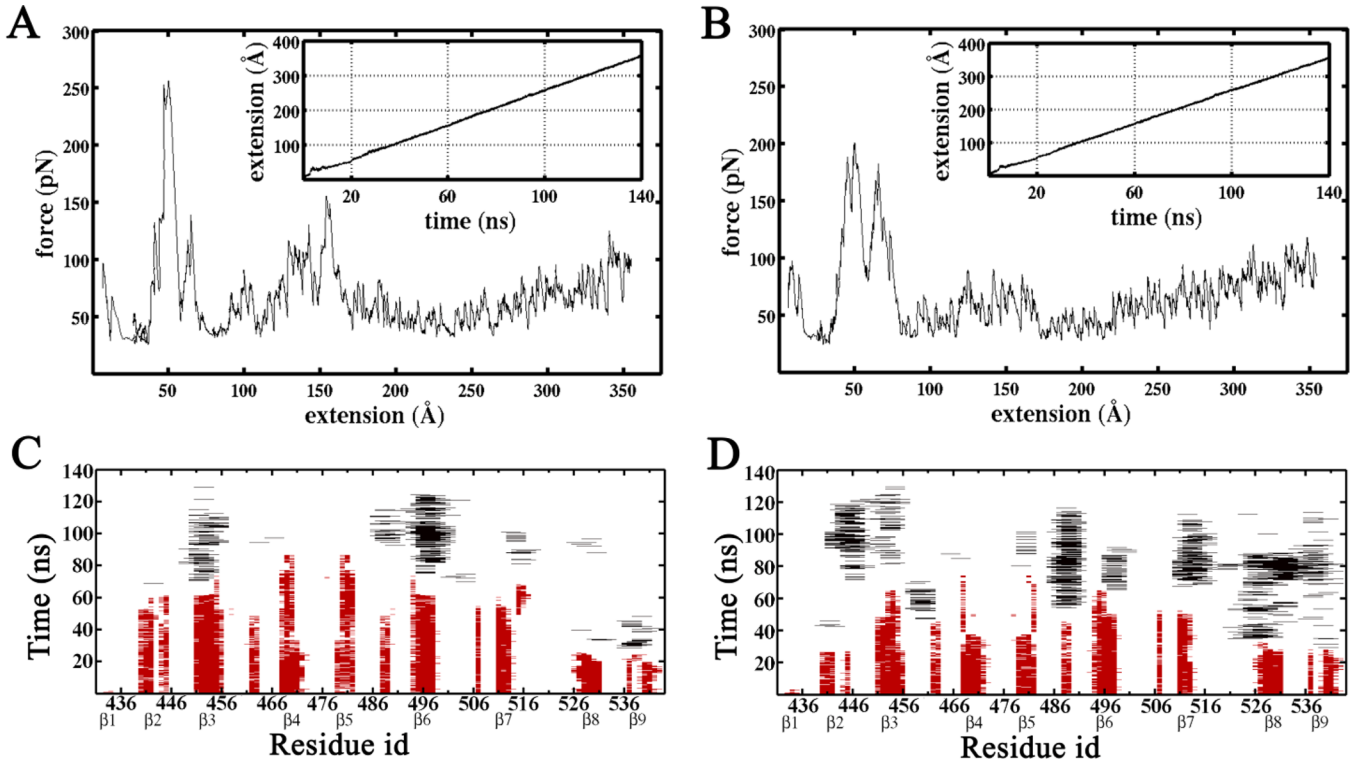

Figure 4. Force−extension curves and secondary structural stability plot for 140 ns of constant velocity steered molecular dynamics (SMD) simulations. Force extension curve for A. wild type lamin Ig fold (with PDB Id 1IFR) and B. for R453W mutant. The corresponding extensions vs time plots have been shown in the inset. First transition was at 50 Å extensions for both wild type and mutant. Transition peaks were at ∼250 and ∼200 pN for the wild type and the mutant, respectively. At 150 Å extension, a comparatively stable intermediate for the wild type (unfolding force of ∼150 pN) was observed than for the mutant with unfolding force ∼75 pN at the same extension). Variations in secondary structures are shown in C, for wild type and D, for R453W mutant. The red and black patches depict respectively beta strand and α helix conformations, of the residues at the corresponding time. The white region represents the unstructured/coil conformation. For the mutant, a clear tendency for the β to α helix transition was observed in later stages of the unfolding. For both the wild type and mutant cases, β1, β8, and β9 strands were less stable. Specifically, for the mutant β2, β4, and β5 strands were very much unstable as compared to that of wild type during the constant velocity SMD simulation.

mutant proteins were performed to indicate the relative stabilities of both the molecules. However, we showed a decrease in number of residues participating in β2 strand for the R453W mutant, although there was no significant difference in contact maps of both the protein during 100 ns simulation. It may be noted that Glu443 and Glu444, both belonging to this β-strand formed a kink in the wild type, which was stabilized by their salt-bridge interaction with Arg453. Because of mutation the salt-bridge was ruptured thereby making these residues unstructured. Steered Molecular Dynamics simulation of both the wild-type and the mutant proteins produced time dependent gradual elongations until the polypeptide chains were completely straightened out and attained maximum extension of ∼350 Å at around 140 ns (Figure 4). Both the forms, however, were shown to retain their shapes and compactness up to 20 ns as obtained from time vs extension plot (Figure 4A and 4B). From the force extension analyses (Figure 4A and 4B), we observed similar kind of unfolding pattern (with two transition peaks) for both wild type and R453W mutant protein. For wild type, the first peak appeared at 50 Å extension corresponding to a force of 250 pN and unfolding force for the latter transition peak, was calculated to be around 150 pN at 150 Å extension. But for the mutant, first transition peak appeared as a doublet between 50 and 75 Å extensions with unfolding force around 200 pN. Interestingly, the mutant exhibited the same peak corresponding to150 Å extension at a lower unfolding force of ∼75 pN. Hence, the mutant R453W was mechanically weaker compared to the wild type as is corroborated from single molecule force spectroscopic data and also from earlier structural studies of the mutant.[9] We analyzed the secondary structure variations of both the wild type and the mutant proteins for the entire simulation trajectories. Since, the first and the last β-strands located at the periphery were hydrogen bonded to each other, and the force was applied parallel to this hydrogen bond vector, β1 at the N-terminal, and β9 at the C-terminal strands were uncoiled at the earliest compared to the other β-strands for both the simulations. This also induced early rupturing of the nearby β8 strand. The simulation trajectories showed significantly different features at short extension (within 180 Å) in the both cases, whereas at longer extensions those domains were almost identical. The variation of different secondary structure elements of all the residues of both the wild-type and mutant protein, with simulation time scale are shown in Figure 4C and Figure 4D. For both the wild type and the mutant, an initial force of ∼100 pN was required to completely rupture the β1-strand at an extension less than 10 Å. A high force of ∼250 and ∼200 pN for the wild type and the mutant proteins respectively corresponded to the disruption of β8−β9 hydrogen bonding and ultimately rupturing of these β-strands. All these events were completed within the first 40 ns of simulation for both the cases. As indicated earlier, the Arg 453 residue of β3 forms two salt-bridges with Glu 443 and Glu 444 of β2, which were lost because of R453W mutation. As a

dx.doi.org/10.1021/bi500726f | *Biochemistry* 2014, 53, 7247−7258

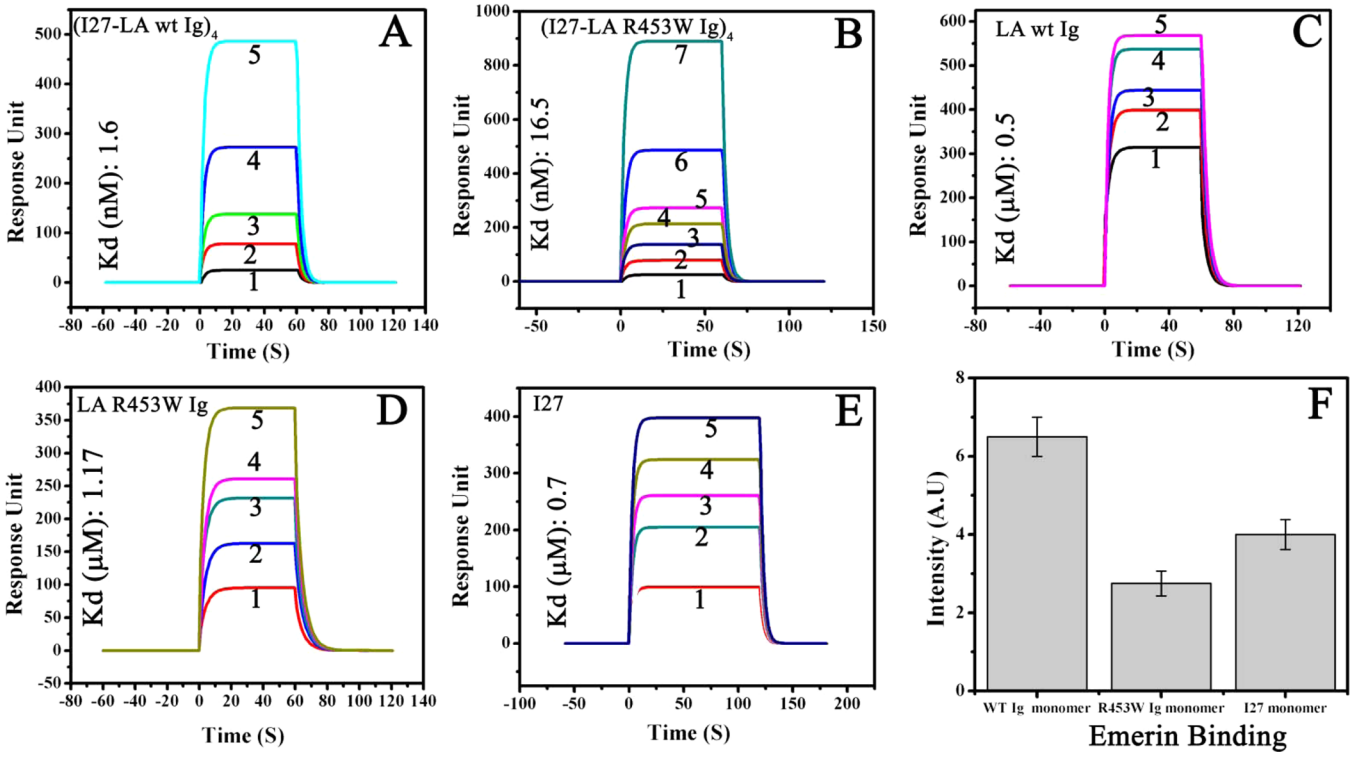

Figure 5. Sensorgrams and dot blot analysis of lamin Ig fold-emerin interaction. Sensorgrams for I27 containing tetrameric proteins and Ig/I27 monomeric constructs were recorded with 0.5 μM and 1.0 μM proteins, respectively. Proteins were immobilized on Ni-NTA chip and emerin was used as analyte. Emerin interaction with $(\text{I27-LA wt Ig})_4$ and $(\text{I27-LA R453W Ig})_4$ cassettes are illustrated in panels A and B respectively, 1−5 depicted emerin of concentrations 0.25, 0.5, 1.0, 2.0, and 4.0 μM in panel A and 1−7 depicted 0.25, 0.5, 1.0, 2.0, 4.0, 8.0, and 12.0 μM for panel B. C, D, and E panels showed the sensograms for the wild type Ig domain monomer, R453W Ig monomer, and I27 monomer, respectively. For each case emerin concentrations were 0.5, 1.0, 1.5, 2.0, and 2.5 μM, which are denoted by the 1 to 5 in the sensograms. All the experiments were carried out in buffer containing 25 mM Tris-HCl (pH 7.4), 150 mM NaCl, at 25 °C. F. Intensity profile of Ig-emerin from dot blot assay, Intensity profiles as obtained from the dot blot assay for the lamin A/C Ig fold-emerin binding were normalized over the background. Wild-type Ig fold showed almost ~2.6 fold higher binding compared to R453W mutant.

Table 2. Binding Affinity of Lamin A Wild Type and R453W Ig Fold and Chimeric $(\text{wt Ig/R453W Ig-I27})_4$ Constructs with Emerin[a]

protein	Ig fold monomer	R453W Ig fold monomer	I27 monomer	wild-type tetramer$(\text{I27-LA wt Ig})_4$	R453W tetramer $(\text{I27-LA R453W Ig})_4$
K_d (nM)	505 ± 42	1170 ± 49	700 ± 53	1.6 ± 0.06	16.5 ± 0.8

[a]Wild type Ig domain has the 2-fold higher affinity for the emerin. All the results were obtained from surface plasmon resonance experiments. K_d,represents the dissociation constant.

result, the β2 strand of the mutant protein was rupturing simultaneously along with β8 and β9 at around the same time indicated by a broader peak at ~50 Å extensions in the force vs extension plot (Figure 4A and Figure 4B). On the other hand, stability of the wild type β2 strand, in comparison to its mutant was higher, as it was completely stretched only after 60 ns and corresponded to a force as high as ~150 pN. Rupturing of β2 was followed by β3 which was again more stable for the wild type as compared to the mutant. The β6 and β7 strands were ruptured next and the process occurred faster in case of mutant protein compared to the wild type under similar conditions of force. The β4 and β5 strands of the first β sheet layer of the wild-type domain remained stable until ~85 ns (up to 200 Å extension) whereas, for the mutant these strands unfolded completely within ~75 ns (up to 150 Å extension) at comparable forces. Similarly, β2 and β7 ruptured quickly in case of mutant protein compared to the wild type under similar conditions. We observed an interesting conformational transition from β-strand to α-helix prior to complete stretching in both the cases. The secondary structure alteration from β-strand to α helix was observed more in case of the mutant-protein. However, the alpha-helices were not stable in either case though their lengths were quite significant. In conclusion the SMD studies are in good agreement with our single molecule force spectroscopy results.

Ig-Fold-Emerin Interaction by SPR and Solid-Phase Binding Assay. Previous results had mapped the interaction of the C-terminal domain of lamin A with emerin.[33] In this study, we investigated whether the R453W mutation in the Ig fold known to cause autosomal dominant EDMD disease alters the binding stability of lamin−emerin complex. We compared the binding affinity of monomeric Ig/tetrameric Ig and the corresponding mutant with emerin by surface plasmon resonance (Figure 5). Lamin Ig fold showed more than 2-fold higher affinities than the corresponding R453W mutant. As we performed the pulling experiments with the tetrameric constructs (i.e., $(\text{I27-LA wt Ig})_4$ and $(\text{I27-LA R453W Ig})_4$) so we intended to look whether emerin binds to this lamin domain

dx.doi.org/10.1021/bi500726f | Biochemistry 2014, 53, 7247−7258

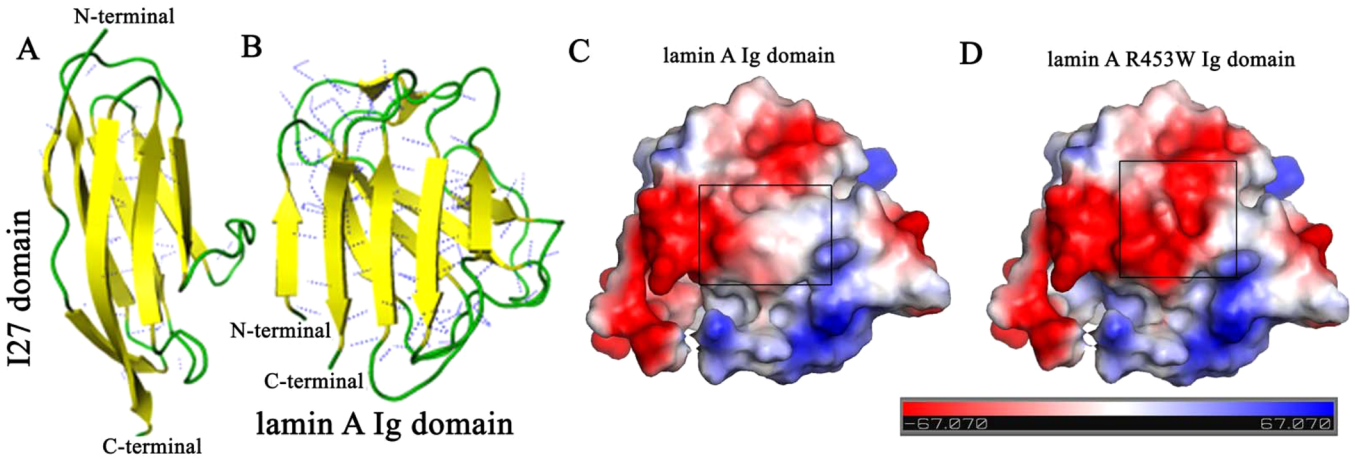

Figure 6. H-bonding geometry of titin I27 domain and lamin A Ig domain and altered surface potential of the mutant domain. A. For titin I27 domain H-bond orientations are in shearing geometry with respect to N- to C-terminal force vector, whereas B. for lamin Ig domain it is in unzipping geometry. C and D are showing the surface potential of the two lamin Ig fold domains. For the mutation R453W, the surface potential of the lamin Ig domain changed dramatically. The electrostatic surface potentials in vacuum were obtained in pymol using APBS tool. Scale bar denotes transition from lower potential to higher potential coded by red and blue, respectively.

also. For these cases also, wild type lamin A Ig domain showed higher binding compared to that of mutant construct. Interestingly I27 also exhibited comparable binding to emerin. It may be noted that, titin was shown to localize in the nuclear envelope during mitosis in C. elegans.[61] The alteration of surface electrostatic potential as a sequel to the mutation R453W might have resulted in 2-fold less binding affinity with emerin. This finding was also corroborated from the solid phase binding analysis by dot blot (Figure 5F) where emerin was found to bind to Ig domain with a stronger affinity compared to R453W Ig. Similar findings were reported earlier by Holt et al. where the sequestration of emerin by ectopically expressed mutant lamin A was dramatically reduced in cultured cell lines.[62] The K_d values calculated from sensorgrams have been shown in Table 2. Therefore, the binding characteristics of Ig fold-emerin were consistent as far as SPR and solid phase analysis were concerned showing that R453W Ig might interact with reduced affinity to the emerin thereby perturbing the mechanotransduction route from cytoskeleton to nucleus.

DISCUSSION

Lamin A Ig domain consists of 113 residues,[9] comprising nine β strands. Two β sheet layers (first sheet of five β strands, 1, 4, 5, 8, and 9 and another set of four strands 2, 3, 6, and 7) are tilted at about 45°, which is a characteristics of lamin β sandwich structure.[8,9] Our results with SMFS showed that (I27-LA R453W Ig)$_4$ unfolded at a lower force compared to (I27-LA wt Ig)$_4$. The mutant unfolded at ∼49 pN force compared to ∼56 pN for the wild type construct. Arg 453 residue makes a classic beta bulge forming two salt bridges with Glu 443 and Glu 444 residues. The R453W mutation abolished these two salt bridges thus making the geometry more facile for unfolding. This result was in excellent agreement with thermal unfolding data. We had also investigated for the first time the time averaged molecular structure of Ig fold and its mutant by equilibrium simulation in the absence of N-to-C terminal directional force where LA wt Ig and LA R453W Ig did not show any difference in RMS fluctuations which meant that both the domains were comparable in their compactness. In this Article, we have gained novel insight into the unfolding signatures of nine beta strands of Ig domain on application of force hitherto not reported. From steered molecular dynamics simulation, we observed there was little mechanical resistance from the first and last two beta strands. Interestingly the mutant yielded a less stable intermediate in the process of unfolding. Similar SMD studies had been reported earlier with the full length tail domain of lamin A by Buehler et. al.[63] By applying replica exchange molecular dynamics they identified the structures of different segments which included mature tail domain and Δ50 tail domain of progerin. 4−5 transition peaks were identified; each corresponded to the unfolding of β-strands requiring large forces (357.8 ± 94.2 pN). This force was more than that obtained from our SMD simulations because that included the entire C-terminal domain as opposed to the Ig fold. Interestingly, lamin Ig fold domain unfolded at lower force than titin I27 domain. Lamin Ig folds yielded to lower force (∼56 pN) compared to the signature elastomeric I27 domain, which unfolded at 200 pN. This could be explained from a closer look at the hydrogen bonding geometry of the two. As comparative mechanical resistance of the biomolecules could be extrapolated from the H-bond geometry with respect to the force vector,[64,65] the terminal β-strands in the lamin Ig domain are antiparallel to one another representing an unzipping geometry while being pulled from N- and C-termini whereas they are parallel and must be unfolded in a shearing geometry in the case of I27 (Figure 6 A and B). The β1 strand was intrinsically destabilized for both wild type and mutant thereby yielding little or no mechanical resistance to pulling. As a result β2−β9 strands effectively contributed for the pulling induced mechanical resistance. It should be emphasized that I27 is a highly elastomeric domain of titin which is a primary effector molecule in generating muscle strength and contraction. On the other hand force transduction to the lamins is attenuated partially by the damping effect of LINC complex and other cytoskeletal filament systems present in the cytoplasm. Therefore, lamin A might be second in the line of response to an external mechanical force.

We also used SMFS to probe the unfolding behavior of the wild type Ig domain and its mutant in the presence of emerin. However, we did not observe any change either in the unfolding behavior or in the contour length of the mutant and the wild type. Interestingly enough, we observed a reduction in

dx.doi.org/10.1021/bi500726f | Biochemistry 2014, 53, 7247−7258

unfolding force of the wild type Ig in the presence of emerin. We could logically conclude that the interaction of emerin with Ig on the surface might entail a conformational change at the core of the molecule which eventually might perturb the hydrogen bonding geometry. On the other hand LA R453W Ig−emerin interaction was not favored presumably because of high electronegative charge buildup on the surface of Ig (Figure 6C and D). Hence, we did not observe any significant change in force compared to the LA R453W Ig alone. This differential interaction of emerin with wild type and mutant Ig was also corroborated from surface plasmon resonance and solid phase binding assays where we observed that emerin bound to lamin Ig fold strongly compared to the mutant domain. Hence, it could be concluded that because of R453W mutation, there was a change in mechanical resistance of the Ig fold domain. This also modified the interactome which includes membrane protein like emerin as in our case. This is quite expected as the electronegative surface potential of the mutant domain would perturb the self-association behavior resulting into aberrant higher order network formation of the mutant protein and also change the interaction profile with other nuclear proteins.

Muscle movements in the human body involve cyclic periodicity of contraction and stretching of the muscle tissues. At the cellular level this translates into alternate waves of tensile strain which is propagated from the exterior of the cell to the nucleus. This transmission of force into the nucleus is mediated by a careful orchestration of LINC protein complexes to the nuclear lamins. Isolated nuclei have been shown to deform reversibly in matter of seconds in response to mechanical stimuli.[66−68] Similar reversible nuclear deformations underlie the stretching and contraction of the myocytes hence muscle tissues. In autosomal dominant EDMD the characteristic viscoelasticity of lamin A network is partially abrogated because of the R453W mutation in the Ig domain which has been shown to stretch at a lower force compared to the wild type. But the probable reason why the nucleus is not grossly deformed due to this mutation might be the compensatory compliance of the lamin B1/B2 network. Another possible outcome of this mutation could also be a modification of the transcriptome, which can exert the effect on the genes involved in the mechanotransduction pathway. At the same time our data has shown a significantly lower affinity of the LA R453W Ig for emerin suggesting a weaker interaction of the lamin A network with emerin ultimately resulting into poor force coupling. Although the LINC complex mediated force transduction could partially occur through nesprin-SUN-lamins route. These two mutually exclusive events summarize the molecular events underlying the pathophysiology of the disease. Therefore, the poor coupling of mechanical stimuli to the nucleoskeleton in connivance with a less compliant network makes the nucleus more vulnerable. Concomitantly, the integrity of the myofibers is seriously sacrificed in response to mechanical stress.

AUTHOR INFORMATION

Corresponding Author

*Phone: 033 2337 5345, ext. 3504. E-mail: kaushik.sengupta@saha.ac.in.

Author Contributions

M.B. and H.C.K. contributed equally

Funding

This work was supported from the BARD project, Department of Atomic energy (DAE), Govt. of India. M.B., H.C.K., A.R., and S.G. thank DAE for intramural fellowships. S.R.K. and K.S.G. thank DAE for intramural grant.

Notes

The authors declare no competing financial interest.

ACKNOWLEDGMENTS

We thank Dr. Frank Bernhard, J.W. Goethe University of Frankfurt and Dr. James Holaska, University of Chicago for the generous gift of pET-21 emerin and pET-15b emerin plasmids, respectively. We also thank Dr. Oishee Chakraborty for the anti-his antibody. We would like to thank Satya Narayan and Anju Yadav of TIFR, Mumbai for their generous help in instrumental set up.

ABBREVIATION

EDMD, Emery−Dreifuss Muscular Dystrophy; SMFS, single-molecule force spectroscopy; LINC, linker of nucleoskeleton and cytoskeleton; SPR, surface plasmon resonance; SMD, steered molecular dynamics

REFERENCES

(1) Fawcett, D. W. (1966) On the occurrence of a fibrous lamina on the inner aspect of the nuclear envelope in certain cells of vertebrates. *Am. J. Anat. 119*, 129−145.

(2) Stuurman, N., Heins, S., and Aebi, U. (1998) Nuclear lamins: Their structure, assembly, and interactions. *J. Struct. Biol. 122*, 42−66.

(3) Herrmann, H., and Foisner, R. (2003) Intermediate filaments: Novel assembly models and exciting new functions for nuclear lamins. *Cell. Mol. Life Sci. 60*, 1607−1612.

(4) Shimi, T., Pfleghaar, K., Kojima, S., Pack, C. G., Solovei, I., Goldman, A. E., Adam, S. A., Shumaker, D. K., Kinjo, M., Cremer, T., and Goldman, R. D. (2008) The A- and B-type nuclear lamin networks: microdomains involved in chromatin organization and transcription. *Genes Dev. 22*, 3409−3421.

(5) Schirmer, E. C., Guan, T., and Gerace, L. (2001) Involvement of the lamin rod domain in heterotypic lamin interactions important for nuclear organization. *J. Cell Biol. 153*, 479−489.

(6) Strelkov, S. V., Schumacher, J., Burkhard, P., Aebi, U., and Herrmann, H. (2004) Crystal structure of the human lamin A coil 2B dimer: implications for the head-to-tail association of nuclear lamins. *J. Mol. Biol. 343*, 1067−1080.

(7) Bhattacharjee, P., Banerjee, A., Banerjee, A., Dasgupta, D., and Sengupta, K. (2013) Structural alterations of Lamin A protein in dilated cardiomyopathy. *Biochemistry 52*, 4229−4241.

(8) Dhe-Paganon, S., Werner, E. D., Chi, Y. I., and Shoelson, S. E. (2002) Structure of the globular tail of nuclear lamin. *J. Biol. Chem. 277*, 17381−17384.

(9) Krimm, I., Ostlund, C., Gilquin, B., Couprie, J., Hossenlopp, P., Mornon, J. P., Bonne, G., Courvalin, J. C., Worman, H. J., and Zinn-Justin, S. (2002) The Ig-like structure of the C-terminal domain of lamin A/C, mutated in muscular dystrophies, cardiomyopathy, and partial lipodystrophy. *Structure 10*, 811−823.

(10) Heitlinger, E., Peter, M., Lustig, A., Villiger, W., Nigg, E. A., and Aebi, U. (1992) The role of the head and tail domain in lamin structure and assembly: Analysis of bacterially expressed chicken lamin A and truncated B2 lamins. *J. Struct. Biol. 108*, 74−89.

(11) Sasse, B., Aebi, U., and Stuurman, N. (1998) A tailless *Drosophila* lamin *Dm*0 fragment reveals lateral associations of dimers. *J. Struct. Biol. 123*, 56−66.

(12) Dittmer, T. A., and Misteli, T. (2011) The lamin protein family. *Genome Biol. 12*, 222.

(13) Shumaker, D. K., Lopez-Soler, R. I., Adam, S. A., Herrmann, H., Moir, R. D., Spann, T. P., and Goldman, R. D. (2005) Functions and

dysfunctions of the nuclear lamin Ig-fold domain in nuclear assembly, growth, and Emery−Dreifuss muscular dystrophy. *Proc. Natl. Acad. Sci. U. S. A. 102*, 15494−15499.
(14) Lammerding, J., Fong, L. G., Ji, J. Y., Reue, K., Stewart, C. L., Young, S. G., and Lee, R. T. (2006) Lamins A and C but not lamin B1 regulate nuclear mechanics. *J. Biol. Chem. 281*, 25768−25780.
(15) Banerjee, A., Rathee, V., Krishnaswamy, R., Bhattacharjee, P., Ray, P., Sood, A. K., and Sengupta, K. (2013) Viscoelastic behavior of human lamin A proteins in the context of dilated cardiomyopathy. *PLoS One 8*, No. e83410.
(16) Crisp, M., Liu, Q., Roux, K., Rattner, J. B., Shanahan, C., Burke, B., Stahl, P. D., and Hodzic, D. (2006) Coupling of the nucleus and cytoplasm: role of the LINC complex. *J. Cell Biol. 172*, 41−53.
(17) Iyer, K. V., Pulford, S., Mogilner, A., and Shivashankar, G. V. (2012) Mechanical activation of cells induces chromatin remodeling preceding MKL nuclear transport. *Biophys. J. 103*, 1416−1428.
(18) Chambliss, A. B., Khatau, S. B., Erdenberger, N., Robinson, D. K., Hodzic, D., Longmore, G. D., and Wirtz, D. (2013) The LINC-anchored actin cap connects the extracellular milieu to the nucleus for ultrafast mechanotransduction. *Sci. Rep. 3*, 1087.
(19) Schirmer, E. C., Florens, L., Guan, T., Yates, J. R., 3rd, and Gerace, L. (2003) Nuclear membrane proteins with potential disease links found by subtractive proteomics. *Science 301*, 1380−1382.
(20) Wilkie, G. S., Korfali, N., Swanson, S. K., Malik, P., Srsen, V., Batrakou, D. G., de las Heras, J., Zuleger, N., Kerr, A. R., Florens, L., and Schirmer, E. C. (2011) Several novel nuclear envelope transmembrane proteins identified in skeletal muscle have cytoskeletal associations. *Mol. Cell Proteomics 10*, No. M110 003129.
(21) Sakaki, M., Koike, H., Takahashi, N., Sasagawa, N., Tomioka, S., Arahata, K., and Ishiura, S. (2001) Interaction between emerin and nuclear lamins. *J. Biochem 129*, 321−327.
(22) Vaughan, A., Alvarez-Reyes, M., Bridger, J. M., Broers, J. L., Ramaekers, F. C., Wehnert, M., Morris, G. E., Whitfield, W. G. F., and Hutchison, C. J. (2001) Both emerin and lamin C depend on lamin A for localization at the nuclear envelope. *J. Cell Sci. 114*, 2577−2590.
(23) Maniotis, A. J., Chen, C. S., and Ingber, D. E. (1997) Demonstration of mechanical connections between integrins, cytoskeletal filaments, and nucleoplasm that stabilize nuclear structure. *Proc. Natl. Acad. Sci. U. S. A. 94*, 849−854.
(24) Martins, R. P., Finan, J. D., Guilak, F., and Lee, D. A. (2012) Mechanical regulation of nuclear structure and function. *Annu. Rev. Biomed Eng. 14*, 431−455.
(25) Clements, L., Manilal, S., Love, D. R., and Morris, G. E. (2000) Direct interaction between emerin and lamin A. *Biochem. Biophys. Res. Commun. 267*, 709−714.
(26) Manilal, S., Nguyen, T. M., and Morris, G. E. (1998) Colocalization of emerin and lamins in interphase nuclei and changes during mitosis. *Biochem. Biophys. Res. Commun. 249*, 643−647.
(27) Capell, B. C., and Collins, F. S. (2006) Human laminopathies: nuclei gone genetically awry. *Nat. Rev. Genet 7*, 940−952.
(28) Raffaele Di Barletta, M., Ricci, E., Galluzzi, G., Tonali, P., Mora, M., Morandi, L., Romorini, A., Voit, T., Orstavik, K. H., Merlini, L., Trevisan, C., Biancalana, V., Housmanowa-Petrusewicz, I., Bione, S., Ricotti, R., Schwartz, K., Bonne, G., and Toniolo, D. (2000) Different mutations in the LMNA gene cause autosomal dominant and autosomal recessive Emery-Dreifuss muscular dystrophy. *Am. J. Hum. Genet. 66*, 1407−1412.
(29) Bonne, G., Mercuri, E., Muchir, A., Urtizberea, A., Becane, H. M., Recan, D., Merlini, L., Wehnert, M., Boor, R., Reuner, U., Vorgerd, M., Wicklein, E. M., Eymard, B., Duboc, D., Penisson-Besnier, I., Cuisset, J. M., Ferrer, X., Desguerre, I., Lacombe, D., Bushby, K., Pollitt, C., Toniolo, D., Fardeau, M., Schwartz, K., and Muntoni, F. (2000) Clinical and molecular genetic spectrum of autosomal dominant Emery−Dreifuss muscular dystrophy due to mutations of the lamin A/C gene. *Ann. Neurol. 48*, 170−180.
(30) Beroud, C., Hamroun, D., Collod-Beroud, G., Boileau, C., Soussi, T., and Claustres, M. (2005) UMD (Universal Mutation Database): 2005 update. *Hum. Mutat. 26*, 184−191.
(31) Dechat, T., Pfleghaar, K., Sengupta, K., Shimi, T., Shumaker, D. K., Solimando, L., and Goldman, R. D. (2008) Nuclear lamins: Major factors in the structural organization and function of the nucleus and chromatin. *Genes Dev. 22*, 832−853.
(32) Taranum, S., Sur, I., Muller, R., Lu, W., Rashmi, R. N., Munck, M., Neumann, S., Karakesisoglou, I., and Noegel, A. A. (2012) Cytoskeletal interactions at the nuclear envelope mediated by nesprins. *Int. J. Cell Biol. 2012*, 736524.
(33) Lee, K. K., Haraguchi, T., Lee, R. S., Koujin, T., Hiraoka, Y., and Wilson, K. L. (2001) Distinct functional domains in emerin bind lamin A and DNA-bridging protein BAF. *J. Cell Sci. 114*, 4567−4573.
(34) Bonne, G., Di Barletta, M. R., Varnous, S., Becane, H. M., Hammouda, E. H., Merlini, L., Muntoni, F., Greenberg, C. R., Gary, F., Urtizberea, J. A., Duboc, D., Fardeau, M., Toniolo, D., and Schwartz, K. (1999) Mutations in the gene encoding lamin A/C cause autosomal dominant Emery-Dreifuss muscular dystrophy. *Nat. Genet. 21*, 285−288.
(35) Scharner, J., Brown, C. A., Bower, M., Iannaccone, S. T., Khatri, I. A., Escolar, D., Gordon, E., Felice, K., Crowe, C. A., Grosmann, C., Meriggioli, M. N., Asamoah, A., Gordon, O., Gnocchi, V. F., Ellis, J. A., Mendell, J. R., and Zammit, P. S. (2011) Novel LMNA mutations in patients with Emery−Dreifuss muscular dystrophy and functional characterization of four LMNA mutations. *Hum. Mutat. 32*, 152−167.
(36) Erber, A., Riemer, D., Hofemeister, H., Bovenschulte, M., Stick, R., Panopoulou, G., Lehrach, H., and Weber, K. (1999) Characterization of the Hydra lamin and its gene: A molecular phylogeny of metazoan lamins. *J. Mol. Evol 49*, 260−271.
(37) Carrion-Vazquez, M., Oberhauser, A. F., Fisher, T. E., Marszalek, P. E., Li, H., and Fernandez, J. M. (2000) Mechanical design of proteins studied by single-molecule force spectroscopy and protein engineering. *Prog. Biophys. Mol. Biol. 74*, 63−91.
(38) Kotamarthi, H. C., Sharma, R., Narayan, S., Ray, S., and Ainavarapu, S. R. (2013) Multiple unfolding pathways of leucine binding protein (LBP) probed by single-molecule force spectroscopy (SMFS). *J. Am. Chem. Soc. 135*, 14768−14774.
(39) Kotamarthi, H. C., Sharma, R., and Koti Ainavarapu, S. R. (2013) Single-molecule studies on PolySUMO proteins reveal their mechanical flexibility. *Biophys. J. 104*, 2273−2281.
(40) Bustamante, C., Marko, J. F., Siggia, E. D., and Smith, S. (1994) Entropic elasticity of lambda-phage DNA. *Science 265*, 1599−1600.
(41) Myszka, D. G., He, X., Dembo, M., Morton, T. A., and Goldstein, B. (1998) Extending the range of rate constants available from BIACORE: Interpreting mass transport-influenced binding data. *Biophys. J. 75*, 583−594.
(42) Phillips, J. C., Braun, R., Wang, W., Gumbart, J., Tajkhorshid, E., Villa, E., Chipot, C., Skeel, R. D., Kale, L., and Schulten, K. (2005) Scalable molecular dynamics with NAMD. *J. Comput. Chem. 26*, 1781−1802.
(43) MacKerell, A. D., Bashford, D., Bellott, M., Dunbrack, R. L., Jr., Evanseck, J. D., Field, M. J., Fischer, S., Gao, J., Guo, H., Ha, S., Joseph-McCarthy, D., Kuchnir, L., Kuczera, K., Lau, F. T. K., Mattos, C., Michnick, S., Ngo, T., Nguyen, D. T., Prodhom, B, Reiher, W. E., III, Roux, B., Schlenrich, M., Smith, J. C., Stote, R., Straub, J., Watanabe, M., Wiórkiewcz-Kuczera, J., Yin, D., and Karplus, M. (1998) All-atom empirical potential for molecular modeling and dynamics studies of proteins. *J. Phys. Chem. B 102*, 3586−3616.
(44) Marti-Renom, M. A., Stuart, A. C., Fiser, A., Sanchez, R., Melo, F., and Sali, A. (2000) Comparative protein structure modeling of genes and genomes. *Annu. Rev. Biophys. Biomol. Struct. 29*, 291−325.
(45) Brooks, B. R., Bruccoleri, R. E., Olafson, B. D., States, D. J., Swaminathan, S., and Karplus, M. (1983) CHARMM: A program for macromolecular energy, minimization, and dynamics calculations. *J. Comput. Chem. 4*, 187−217.
(46) Izrailev, S., Stepaniants, S., Balsera, M., Oono, Y., and Schulten, K. (1997) Molecular dynamics study of unbinding of the avidin-biotin complex. *Biophys. J. 72*, 1568−1581.
(47) Evans, E., and Ritchie, K. (1997) Dynamic strength of molecular adhesion bonds. *Biophys. J. 72*, 1541−1555.

(48) Balsera, M., Stepaniants, S., Izrailev, S., Oono, Y., and Schulten, K. (1997) Reconstructing potential energy functions from simulated force-induced unbinding processes. *Biophys. J. 73*, 1281−1287.
(49) Feig, M., and Brooks, C. L., 3rd. (2004) Recent advances in the development and application of implicit solvent models in biomolecule simulations. *Curr. Opin Struct Biol. 14*, 217−224.
(50) Guvench, O., Weiser, J., Shenkin, P., Kolossvary, I., and Still, W. C. (2002) Application of the frozen atom approximation to the GB/SA continuum model for solvation free energy. *J. Comput. Chem. 23*, 214−221.
(51) Qiu, D., Shenkin, P. S., Hollinger, F. P., and Still, W. C. (1997) The GB/SA continuum model for solvation. A fast analytical method for the calculation of approximate Born radii. *J. Phys. Chem. A 101*, 3005−3014.
(52) Kabsch, W., and Sander, C. (1983) Dictionary of protein secondary structure: Pattern recognition of hydrogen-bonded and geometrical features. *Biopolymers 22*, 2577−2637.
(53) Oberhauser, A. F., Marszalek, P. E., Carrion-Vazquez, M., and Fernandez, J. M. (1999) Single protein misfolding events captured by atomic force microscopy. *Nat. Struct. Biol. 6*, 1025−1028.
(54) Marszalek, P. E., Lu, H., Li, H., Carrion-Vazquez, M., Oberhauser, A. F., Schulten, K., and Fernandez, J. M. (1999) Mechanical unfolding intermediates in titin modules. *Nature 402*, 100−103.
(55) Brockwell, D. J., Beddard, G. S., Clarkson, J., Zinober, R. C., Blake, A. W., Trinick, J., Olmsted, P. D., Smith, D. A., and Radford, S. E. (2002) The effect of core destabilization on the mechanical resistance of I27. *Biophys. J. 83*, 458−472.
(56) Li, H., Carrion-Vazquez, M., Oberhauser, A. F., Marszalek, P. E., and Fernandez, J. M. (2000) Point mutations alter the mechanical stability of immunoglobulin modules. *Nat. Struct. Biol. 7*, 1117−1120.
(57) Buxboim, A., Ivanovska, I. L., and Discher, D. E. (2010) Matrix elasticity, cytoskeletal forces and physics of the nucleus: how deeply do cells 'feel' outside and in? *J. Cell Sci. 123*, 297−308.
(58) Holaska, J. M. (2008) Emerin and the nuclear lamina in muscle and cardiac disease. *Circ. Res. 103*, 16−23.
(59) Stewart, C. L., Roux, K. J., and Burke, B. (2007) Blurring the boundary: the nuclear envelope extends its reach. *Science 318*, 1408−1412.
(60) Zwerger, M., Jaalouk, D. E., Lombardi, M. L., Isermann, P., Mauermann, M., Dialynas, G., Herrmann, H., Wallrath, L. L., and Lammerding, J. (2013) Myopathic lamin mutations impair nuclear stability in cells and tissue and disrupt nucleo-cytoskeletal coupling. *Hum. Mol. Genet. 22*, 2335−2349.
(61) Zastrow, M. S., Flaherty, D. B., Benian, G. M., and Wilson, K. L. (2006) Nuclear titin interacts with A- and B-type lamins in vitro and in vivo. *J. Cell Sci. 119*, 239−249.
(62) Holt, I., Ostlund, C., Stewart, C. L., Man, N., Worman, H. J., and Morris, G. E. (2003) Effect of pathogenic mis-sense mutations in lamin A on its interaction with emerin in vivo. *J. Cell Sci. 116*, 3027−3035.
(63) Qin, Z., Kalinowski, A., Dahl, K. N., and Buehler, M. J. (2011) Structure and stability of the lamin A tail domain and HGPS mutant. *J. Struct. Biol. 175*, 425−433.
(64) Brockwell, D. J., Paci, E., Zinober, R. C., Beddard, G. S., Olmsted, P. D., Smith, D. A., Perham, R. N., and Radford, S. E. (2003) Pulling geometry defines the mechanical resistance of a β-sheet protein. *Nat. Struct. Biol. 10*, 731−737.
(65) Keten, S., and Buehler, M. J. (2008) Strength limit of entropic elasticity in β-sheet protein domains. *Phys. Rev. E: Stat., Nonlinear, Soft Matter Phys. 78*, No. 061913.
(66) Guilak, F., Tedrow, J. R., and Burgkart, R. (2000) Viscoelastic properties of the cell nucleus. *Biochem. Biophys. Res. Commun. 269*, 781−786.
(67) Rowat, A. C., Lammerding, J., and Ipsen, J. H. (2006) Mechanical properties of the cell nucleus and the effect of emerin deficiency. *Biophys. J. 91*, 4649−4664.
(68) Vaziri, A., and Mofrad, M. R. (2007) Mechanics and deformation of the nucleus in micropipette aspiration experiment. *J. Biomech. 40*, 2053−2062.